JOM
https://doi.org/10.1007/s11837-018-2856-6

Fast Slip Velocity in a High-Entropy Alloy

Q. RIZZARDI,[1] G. SPARKS,[1] and R. MAAß[1,2]

1.—Department of Materials Science and Engineering and Frederick Seitz Materials Research Laboratory, University of Illinois at Urbana-Champaign, Champaign, IL 61801, USA. 2.—e-mail: rmaass@illinois.edu

Due to fluctuations in nearest-neighbor distances and chemistry within the unit cell, high-entropy alloys are believed to have a much higher resistance to dislocation motion than pure crystals. Here, we investigate the coarse-grained dynamics of a number of dislocations being active during a slip event. We found that the time-resolved dynamics of slip is practically identical in Au⟨001⟩ and an $Al_{0.3}$CoCrFeNi⟨001⟩ high-entropy alloy, but much faster than in Nb⟨001⟩. Differences between the FCC-crystals are seen in the spatiotemporal velocity profile, with faster acceleration and slower velocity relaxation in the high-entropy alloy. Assessing distributions that characterize the intermittently evolving plastic flow reveals material-dependent scaling exponents for size, duration, and velocity–size distributions. The results are discussed in view of the underlying dislocation mobility.

INTRODUCTION

Crystal plasticity, and thus mechanical strength, has always been a topic much guided by translating dislocation mechanisms and dislocation properties into how a crystal responds plastically to a far field stress. This also applies to the novel group of so-called high-entropy alloys (HEA), or more generally alloy systems in which the concept of multi-principal elements is exploited.[1] One prominent aspect of this class of alloys is that chemical fluctuations are present in the unit cell, introducing fluctuations in nearest-neighbor distances and chemistry along different lattice vectors. The precise quantification of the lattice distortion effect is a demanding task, and may be done with advanced x-ray methods[2–5] or high-resolution transmission electron microscopy.[6–8] Indeed, a recent study by Raabe and co-workers used x-ray absorption fine-structure spectroscopy which revealed a small lattice mean distortion of the order of 0.1%, and that local fluctuations may be as large as ± 5%.[3] Furthermore, transmission electron microscopy evidenced 2–4-nm large regions of distorted lattice that indicate some internal length-scale of the lattice beyond the size of the unit cell.[7,8] Based on such distortions, specific material properties and their temperature dependencies are often explained. This includes mechanical properties, such as hardness,[2,5] yield strength,[6] or strain rate sensitivity.[9] Physically, this is appealing, as one expects strong local fluctuations in the Peierls potential, or, more generally, in the activation energy of a general Arrhenius form for dislocation velocity, both of which are expected to affect the mobility of dislocations.[10,11]

In order to substantiate a reduced dislocation mobility in experiments, one would need to trace line defects in real time or conduct etch pit measurements, the latter of which have provided our experimental database for velocities of both individual dislocations and groups of dislocations.[12] None of these experimental avenues are straightforward and first require a deeper understanding of line defects in HEA, which is currently gained from scanning electron microscopy,[13] transmission electron microcopy[14–17] and atomistic simulations.[18–21] In particular, recent simulations on a concentrated solid-solution NiFe-alloy, serving as a HEA model system, paid attention to the drag coefficient of dislocation motion, revealing that the movement in NiFe compared to pure Ni is strongly damped.[19] The up to 10-times higher damping coefficient led to the conclusion of highly reduced dislocation velocities in HEAs relative to dislocations in single-element metals. Furthermore, large fluctuations in the mobility were observed at different parts of the lattice, again underlining the significance of local lattice distortions and local chemical fluctuations.

Published online: 17 April 2018

Here, we aim to contribute to the discussion on deformation dynamics of HEAs by exploiting an experimental approach that traces in real time the dynamics of crystallographic slip with nano-scale resolution.[22–24] This method is based on a nanoindentation platform used to conduct the well-known micro-compression experiment.[25] Instead of focusing on the general stress–strain behavior of microcrystals, we pay attention to the glide velocity measured during intermittent plasticity, which has been shown to be measurable.[22] This slip velocity corresponds to a net Burger's vector content that is deposited onto the surface at a given rate, thereby generating crystallographic slip. We are thus monitoring a coarse-grained response of the overall dislocation activity on glide plane(s) during a force–displacement instability. Specifically, we investigate the slip-dynamics of an $Al_{0.3}$CoCrFeNi-alloy (FCC) in comparison with pure gold and niobium crystals. The main finding of this assessment is that there is statistically no difference in peak velocities of slip between the HEA and pure gold.

EXPERIMENTAL METHODS

Micro-compression experiments were performed on the following three types of crystals: pure Au (FCC), pure Nb (BCC), and the HEA $Al_{0.3}$CoCrFeNi prepared as outlined in Ref. 26. All the elements in the HEA apart from aluminum have equal stoichiometric ratios; the HEA alloy crystallizes in an FCC structure.[27] The samples are oriented for compression along the [001]-direction and of cylindrical shape with a nominal diameter of 2 μm and a height of 6 μm. We used the same focused-ion beam preparation protocol as in Refs. 24 and 28. Small-scale mechanical testing was carried out using a TI-950 nanoindentation platform, as described in Ref. 22. The experiments for Au and Nb crystals were carried out in displacement-controlled mode and the following rates were applied: 60 nm/s for Au, and 0.6 nm/s for Nb. The reason for the difference in rates is twofold: (1) slip in Nb is ca. 1.5 orders of magnitude slower, and, in order to keep the applied rate below the slip velocity, the displacement rate needs to be reduced; and (2) the FCC crystals cannot be tested at the same low displacement rate, since the events are rapid and need to be recorded with a high sampling rate under the constraint that the device has a limited number of data points that it can store. Despite the differences in rate, the presented results are unaffected by the drive rate, which we have explored across seven orders of displacement rate for Nb. As for the HEA, while displacement control would allow a better regulation of the strain rate, due to the greater magnitude of event sizes observed in the HEA, open-loop control was used to avoid the unloading-reloading dead times that occur after large events in displacement control, allowing for an increased data acquisition rate and improved tracking of the very fast events. Previous experiments have shown that the change of loading mode on the same indentation platform does not significantly affect the event statistics.[29] In order to reduce noise, Wiener filtering was applied to the raw displacement data. The resulting data were analyzed through custom Matlab routines and Python scripts using the following packages: *scipy*, *matplotlib*, *os* and *powerlaw*.[30] The final exploitable datasets are the force applied by the transducer at the slip event, the event duration, the slip-event size as axial displacement of the transducer (compression of the pillar), and the time-resolved slip-velocity profile. Figure 1 displays a typical force–displacement curve, together with a zoom-in onto the precise time-resolved displacement and velocity data, and also defines the extracted peak velocity of a slip event. All statistics presented in this paper are drawn from these variables (with the addition of applied force). Estimations of power-law exponents and fits of distribution functions are obtained by the maximum likelihood estimator (MLE) method. Variations of the power-law exponent as a function of the chosen data range of the complementary cumulative distribution function (CCDF) have been carried out to optimize the fit. For that optimal range, other fits were also applied and compared to the truncated power-law fit, including a power-law, an exponential, a stretched exponential, and a lognormal distribution.

RESULTS AND DISCUSSION

We begin with a comparison of the force at which each slip event occurs and the event sizes (Fig. 2). In the following, the presented datasets include 1449, 162, and 242 events for Au, the HEA, and Nb, respectively. While there is overlap between all three crystals in the event-size range covered, there

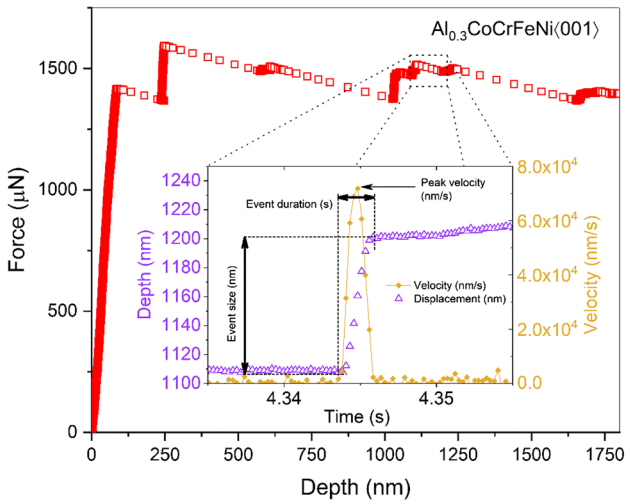

Fig. 1. A typical force–displacement curve obtained from $Al_{0.3}$CoCrFeNi⟨001⟩. The inset highlights the time-resolved displacement–time and velocity–time data used during the analysis.

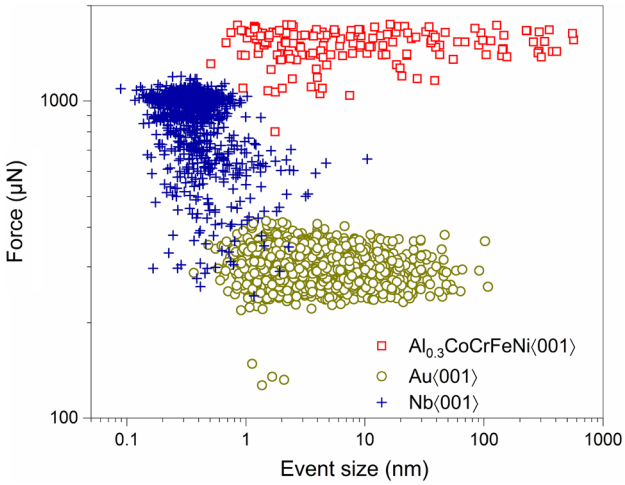

Fig. 2. Applied force at the slip event as a function of subsequent slip size Au⟨001⟩, Nb⟨001⟩, and $Al_{0.3}$CoCrFeNi⟨001⟩.

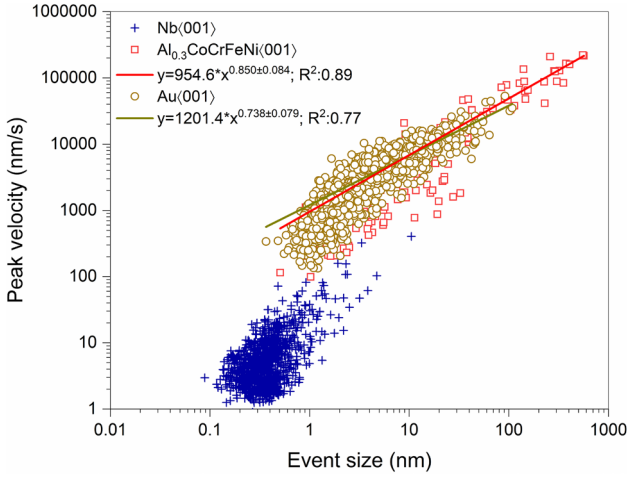

Fig. 3. Peak slip-velocity as a function of event size velocity-size event distributions for Au⟨001⟩, Nb⟨001⟩, and $Al_{0.3}$CoCrFeNi⟨001⟩. Power-law fits have been applied to the Au and the HEA-alloy data.

is a clear trend for the Nb crystal to present smaller events. Both Au and the HEA show a similar lower range at approx. 0.5 nm for their smaller events, but almost an order of magnitude larger slip events can be recorded for the HEA. The distinct force levels of the data in Fig. 2 reflect the different flow stresses of the crystals ($\sim$ 65–125 MPa for Au, 95–320 MPa for Nb, and $\sim$ 380–600 MPa for the HEA), where the larger spread in the Nb data is due to repeated load–unload segments that allow probing smaller stress scales upon reloading. The load–unload cycles were needed so as to strain the crystal to the same extent ($\sim$ 20% engineering strain) under the constraint of a low displacement rate and a finite buffer size of the instrument. Figure 2 displays that, once the applied force is sufficient to trigger a collective dislocation event, any value of slip-size magnitude can be obtained.

The peak velocity (see Fig. 1 for definition) of the events as a function of their size is summarized in Fig. 3. A clear distinction can be made between, on the one side, Au and the HEA with fast slip dynamics ranging approx. from 100 to 10^5 nm/s, and on the other side, Nb that shows generally slower slip velocities ranging from 1 to 10^3 nm/s. Given the data trends for both Au and the HEA, we apply a power-law fit of type $y = ax^b$ (R^2 = 0.77 for Au, R^2 = 0.89 for the HEA) to the data. For both crystal types, the trend gives a value of b for Au and HEA of 0.74 $\pm$ 0.079 and 0.85 $\pm$ 0.084, respectively, which shows a great degree of similarity and overlapping confidence intervals. Clearly, the same is not observed for Nb and a coefficient of determination less than 0.4 is obtained. Thus, crystallographic slip mediated by avalanches proceeds on average at similar velocity in the HEA and in the Au for events of similar size, which means that the total number of dislocations ($\sim$ 25 dislocations for a typical shear-offset of 5 nm, using the Burgers vector of 0.288 nm for Au) deposited onto the crystal surface is approximately the same.

In the spirit of earlier studies,[29,31–33] we constructed the CCDF of the slip sizes (Fig. 4). The data in Fig. 4 were tested against a pure power-law and a truncated power-law $C(S) \propto S^{-\tau}e^{\lambda S}$, where S is the event size, τ is the fitted exponent, and λ is some non-universal constant that may be linked to finite size effects, strain hardening capability or device stiffness.[34] Using the MLE package (see Experimental section), we observe that the event-size distributions are best described by a truncated power-law. Other types of distributions, such as an exponential, stretched exponential, or a lognormal distribution, do not describe the data well. Table I summarizes the fitting results from the MLE analysis. It is noted that the precise exponents differ distinctly between the materials, which urges the question as to how universal scaling exponents for event-size distributions obtained from intermittent plasticity are. The MLE analysis returns the parameters R ratio (log of likelihood ratio) and p value (significance), both of which give a quantitative measure of a comparison between a power-law and a truncated power-law fit. As seen in Table I, the R ratio is negative for all crystals, therefore favoring a truncated power-law over the pure power-law, which indicates a finite dislocation–dislocation correlation length typical for dislocation network entanglement.[35] This distinction is less strong for the HEA even though the truncated power-law is still the better model. The same insight is gained from the p values, as listed in Table I.

The same CCDF was established for the slip-size durations (not shown here). The Au and HEA crystals cover remarkably similar values in their distribution, with event durations between 0.5×10^{-4} s and 10^{-2} s. In combination with the data in Fig. 3, this shows that events of similar size also have very similar durations in these two materials. Therefore, we conclude that

crystallographic slip, mediated by the same net Burgers vector content, is proceeding statistically identically in both pure Au and the HEA. Since our experiments do not trace the mobility of individual dislocations, a direct link to the underlying dislocation mobility is lacking. However, the similar slip dynamics suggests an almost equivalent rate of dislocations reaching the sample surface. Either the dead time between single Burgers vectors being deposited onto the surface is much larger in Au than in the HEA, or there is simply no significant difference between the velocities of dislocations in both crystals at the probed stress. In the case of Nb, on the other hand, there is a distinct difference: a slip of much smaller net displacements than for Au and the HEA (Fig. 3) occurs during times that are on average ca. 1.5 orders of magnitude longer. Even the longest durations measured for both Au and HEA are smaller than the shortest slip durations seen for Nb. There is thus a clear demarcation between slip-velocities of the FCC crystal structure (Au and HEA) and the BCC represented by Nb, which is predominantly caused by both the time it takes to generate a slip offset of a given size and the generally smaller slip distances in Nb.

Tracing the crystallographic slip dynamics in real time also allows the assessing of the full velocity profile during slip. Similarly as for the event-size distributions, there are various theoretical predictions for the average shape of these profiles.[36–38] These functions have the general form $\langle v \rangle_t = Ate^{-Bt^c}$, where A and B are some constants, and the exponent c describes the velocity decay of the average shape function. In Ref. 36, c was predicted to be 2, for the case of a profile that is rescaled by $S^{-0.5}$ in both velocity and time. We use this scaling and average all individual profiles across all event sizes to obtain the experimental average shape-function of the slip dynamics (Fig. 5). The corresponding fitting results are summarized in Table II. Due to the substantially different time scales of the slip-dynamics in Nb in comparison to the FCC crystals, the size-integrated velocity profile is depicted as an inset in Fig. 5. The different averaged velocity profiles reveal materials-

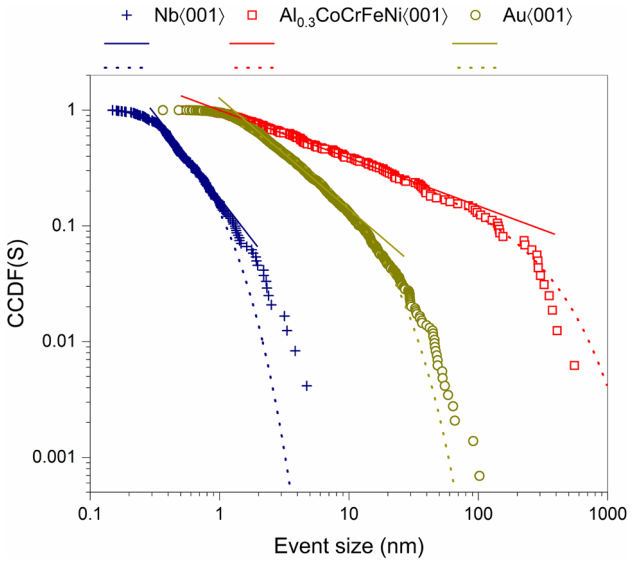

Fig. 4. CCDF distribution of event sizes for Au⟨001⟩, Nb⟨001⟩, and $Al_{0.3}$CoCrFeNi⟨001⟩. The solid line fit is the power law, while the dotted line fit represents the truncated power law.

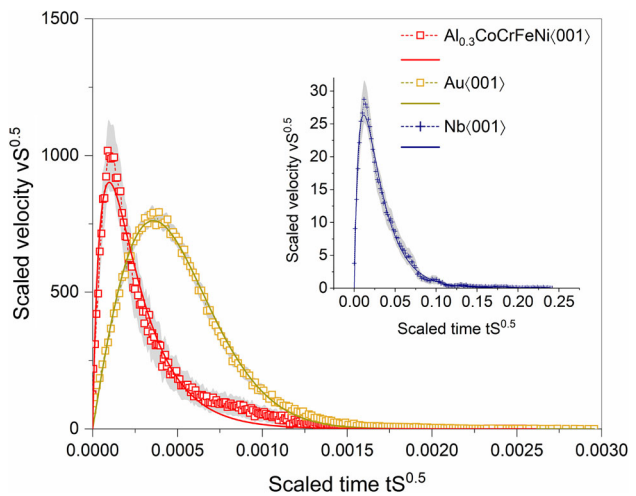

Fig. 5. Size-integrated slip-velocity profiles for Au⟨001⟩, Nb⟨001⟩, and $Al_{0.3}$CoCrFeNi⟨001⟩. The solid lines are fitting curves following $v_t = Ate^{-Bt^c}$. Error bars (standard error of the mean) of the averaged profiles are indicated with gray shaded background.

Table I. Value of exponents found for power-law and truncated power-law fits for Au⟨001⟩, Nb⟨001⟩, and $Al_{0.3}$CoCrFeNi⟨001⟩

	Exponent PL	Exponent truncated PL	*R* Ratio	*p* value
Au⟨001⟩	0.967	1.590	− 5.631	3.33×10^{-16}
$Al_{0.3}$CoCrFeN⟨001⟩	0.437	1.220	− 3.716	1.97×10^{-6}
Nb⟨001⟩	1.530	2.237	− 0.842	0.164

R Ratio is a comparison of both fits; a $R > 0$ value favors power-law, and $R < 0$ favors truncated PL. A significant p value (< 0.05) means that the favored fit is significantly better indicated for the given distribution.

Table II. Fitting parameters and R^2 value of $\langle v \rangle_t = Ate^{-Bt^c}$ for the data displayed in Fig. 5

	A	B	C	R^2
Au⟨001⟩	$3.85 \times 10^6 \pm 1.05 \times 10^5$	$3.75 \times 10^5 \pm 1.18 \times 10^5$	1.68 ± 0.045	0.99
$Al_{0.3}$CoCrFeNi⟨001⟩	$3.70 \times 10^7 \pm 3.71 \times 10^6$	$1.20 \times 10^3 \pm 2.93 \times 10^2$	0.73 ± 0.034	0.98
Nb⟨001⟩	$8.67 \times 10^3 \pm 7.67 \times 10^2$	38.0 ± 2.93	0.75 ± 0.031	0.99

dependent velocity decays, as represented by the exponent. The slip-dynamics in the Au crystal yields the best fit with an exponent of 1.68, which is not too far from the value of 2 that is predicted by mean-field theory for avalanches near the depinning transition.[36] This is not the case for the other crystals, even though the re-scaling and averaging yields a well-defined profile, which indicates that, even though the underlying assumption of $\langle V_{peak} \rangle \propto S^{0.5}$ is not explicitly met (Fig. 3), a correspondingly scaled and averaged profile can be obtained. The velocity decay of the HEA-alloy proceeds more slowly, and is best described with an exponent of 0.73. Fitting the velocity profile of the HEA-alloy with c constrained to 2 yields a significantly decreased fitting quality ($R^2 = 0.82$). The Nb crystal with the slowest slip dynamics in terms of peak velocities has a similar slow velocity decay as the HEA alloy with an exponent of 0.75. Again, constraining the exponent to 2 returns a worse fit, with $R^2 = 0.80$. Also during slip acceleration, the Au and HEA exhibit differences, with HEA reaching the peak velocity significantly faster than Au, which is displayed well in the unscaled velocity profiles (not shown here) or seen by the fitting results in Table II. After reaching the peak velocity, the HEA decays more quickly than Au, but exhibits a final portion of the scaled profile that has a slow deceleration until zero velocity is reached at approximately the same scaled time as for Au. These subtle features suggest on average different rates of slip-displacement creation, which is linked to the rates at which dislocation segments reach the crystal surface. Due to the small crystal size, we assume that the slip is primarily created by dislocations leaving the crystal. We thus observe that the averaged and time-resolved slip dynamics is described by three distinctly different velocity-profiles.

CONCLUSION

In this study, we have statistically investigated properties describing crystallographic slip dynamics in deforming microcrystals, with the particular interest in comparing slip in a pure Au⟨001⟩ crystal and an FCC HEA alloy ($Al_{0.3}$CoCrFeNi⟨001⟩). Nb⟨001⟩ was included in this comparison as to display dramatic differences between crystal systems, where the much slower slip dynamics in Nb is attributed to the rate-limiting motion of the underlying screw dislocation mobility.[39] Our data reveal that slip proceeds statistically with the same peak velocity in both the Au and the HEA at their respective flow stress, irrespective of slip magnitude. At the coarse-grained level of our experiment, no evidence for a distinctly different defect mobility can thus be revealed. The origin of this may be explained with an unresolvable difference in deposition rate of dislocations onto the surface, if indeed the HEA has a significantly lower dislocation mobility. With the lack of detailed insights into the mobility of dislocation in HEAs, it is only possible to extrapolate from simulations to seek an explanation for the similar slip dynamics in both FCC systems. To this end, we consider the insights gained from Nöhring, who explored barrier energies of cross-slip in random alloys.[40] It was found that long dislocations with too high barriers to be overcome by thermal activation alone can cross-slip at a rate orders of magnitude faster than expected. Under stress, cross-slip was shown to become a weakest-link problem, as a small cross-slipped segment could expand spontaneously after nucleation. Whilst it is clear that the depinning stress for dislocations in HEA is higher than in a regular FCC lattice (as also seen by the higher critical stresses to initiate a dislocation avalanche), it may thus be that the mobility of the dislocation in motion is rather dominated by a similar weakest-link scenario as long as the applied stress is high enough for depinning. In this case, shallow barriers along the dislocation line may become rate-limiting for glide. Future research will clarify if this is the case. Our experiments at this stage only reveal differences in the shape of the time-resolved velocity profiles, but not between the peak velocities.

ACKNOWLEDGEMENTS

This research was carried out in part in the Frederick Seitz Materials Research Laboratory Central Research Facilities, University of Illinois. G.S. and R.M. especially thank Kathy Walsh for experimental support with the Hysitron TriboIndenter. R.M. would like to thank P.M. Derlet for fruitful discussions, and is grateful for financial support by the NSF CAREER program (grant NSF DMR 1654065), and for start-up funds provided by the Department of Materials Science and Engineering at UIUC. The authors also thank P. Liaw for providing the HEA.

REFERENCES

1. D.B. Miracle and O.N. Senkov, *Acta Mater.* 122, 448 (2017).

2. J.W. Yeh, *Annales de Chimie Science des Materiaux (Paris)* 31, 633 (2006).
3. H. Oh, D. Ma, G. Leyson, B. Grabowski, E. Park, F. Körmann, and D. Raabe, *Entropy* 18, 321 (2016).
4. J.W. Yeh, S.K. Chen, J.Y. Gan, S.J. Lin, T.S. Chin, T.T. Shun, C.H. Tsau, and S.Y. Chang, *Metall. Mater. Trans. A* 35A, 2533 (2004).
5. B.S. Murty, J.W. Yeh, and S. Ranganathan, *High-Entropy Alloys*, 1st edn. Elsevier.
6. S. Maiti and W. Steurer, *Acta Mater.* 106, 87 (2016).
7. Y. Zou, S. Maiti, W. Steurer, and R. Spolenak, *Acta Mater.* 65, 85 (2014).
8. J.C. Rao, V. Ocelík, D. Vainchtein, Z. Tang, P.K. Liaw, and J.T.M. De Hosson, *Rev. Adv. Mater. Sci.* 48, 105 (2017).
9. A.V. Podolskiy, E.D. Tabachnikova, V.V. Voloschuk, V.F. Gorban, N.A. Krapivka, and S.A. Firstov, *Mater. Sci. Eng. A* 710, 136 (2018).
10. S. Yoshida, T. Bhattacharjee, Y. Bai, and N. Tsuji, *Scripta Mater.* 134, 33 (2017).
11. Y.Y. Zhao and T.G. Nieh, *Intermetallics* 86, 45 (2017).
12. H. Neuhäuser, *Dislocations Solids* 6, 319 (1983).
13. T.K. Liu, Z. Wu, A.D. Stoica, Q. Xie, W. Wu, Y.F. Gao, H. Bei, and K. An, *Mater. Des.* 131, 419 (2017).
14. F. Otto, A. Dlouhý, C. Somsen, H. Bei, G. Eggeler, and E.P. George, *Acta Mater.* 61, 5743 (2013).
15. Q. Lin, X. An, H. Liu, Q. Tang, P. Dai, and X. Liao, *J. Alloys Compd.* 709, 802 (2017).
16. J. Liu, C. Chen, Y. Xu, S. Wu, G. Wang, H. Wang, Y. Fang, and L. Meng, *Scr. Mater.* 137, 9 (2017).
17. J. Miao, C.E. Slone, T.M. Smith, C. Niu, H. Bei, M. Ghazisaeidi, G.M. Pharr, and M.J. Mills, *Acta Mater.* 132, 35 (2017).
18. S.I. Rao, C. Woodward, T.A. Parthasarathy, and O. Senkov, *Acta Mater.* 134, 188 (2017).
19. S. Zhao, Y.N. Osetsky, and Y. Zhang, *J. Alloys Compd.* 701, 1003 (2017).
20. W.G. Nöhring and W.A. Curtin, *Acta Mater.* 128, 135 (2017).
21. S. Zhao, G.M. Stocks, and Y. Zhang, *Acta Mater.* 134, 334 (2017).
22. G. Sparks, P.S. Phani, U. Hangen, and R. Maass, *Acta Mater.* 122, 109 (2017).
23. R. Maass, P.M. Derlet, and J.R. Greer, *Small* 11, 341 (2015).
24. R. Maass, P.M. Derlet, and J.R. Greer, *Scr. Mater.* 69, 586 (2013).
25. M.D. Uchic and D.M. Dimiduk, *Mater. Sci. Eng., A* 400–401, 268 (2005).
26. R.X. Li, P.K. Liaw, and Y. Zhang, *Mater. Sci. Eng. A* 707, 668 (2017).
27. W.-R. Wang, W.-L. Wang, S.-C. Wang, Y.-C. Tsai, C.-H. Lai, and J.-W. Yeh, *Intermetallics* 26, 44 (2012).
28. R. Maass, C.A. Volkert, and P.M. Derlet, *Scr. Mater.* 102, 27 (2015).
29. R. Maass, M. Wraith, J.T. Uhl, J.R. Greer, and K.A. Dahmen, *Phys. Rev. E* 91, 042403 (2015).
30. J. Alstott, E. Bullmore, and D. Plenz, *PLoS One* 9 (4), e95816 (2014). https://doi.org/10.1371/journal.pone.0085777.
31. D.M. Dimiduk, C. Woodward, R. LeSar, and M.D. Uchic, *Science* 312, 1188 (2006).
32. M. Zaiser, J. Schwerdtfeger, A.S. Schneider, C.P. Frick, B.G. Clark, P.A. Gruber, and E. Arzt, *Phil. Mag.* 88, 3861 (2008).
33. N. Friedman, A.T. Jennings, G. Tsekenis, J.-Y. Kim, M. Tao, J.T. Uhl, J.R. Greer, and K.A. Dahmen, *Phys. Rev. Lett.* 109, 095507 (2012).
34. F.F. Csikor, C. Motz, D. Weygand, M. Zaiser, and S. Zapperi, *Science* 318, 251 (2007).
35. R. Maass and P.M. Derlet, *Acta Mater.* 143, 338 (2018).
36. J. Antonaglia, W.J. Wright, X. Gu, R.R. Byer, T.C. Hufnagel, M. LeBlanc, J.T. Uhl, and K.A. Dahmen, *Phys. Rev. Lett.* 112, 155501 (2014).
37. M. LeBlanc, L. Angheluta, K. Dahmen, and N. Goldenfeld, *Phys. Rev. E Stat. Nonlinear Soft Matter Phys.* 87, 022126 (2013).
38. A. Dobrinevski, P. Le Doussal, and K.J. Wiese, *EPL (Europhysics Letters)* 108, 66002 (2014).
39. G. Sparks and R. Maass, *Acta Mater.* (2018). https://doi.org/10.1016/j.actamat.2018.04.007.
40. W.G. Nöhring, *Dislocation Cross-Slip in Face-Centered Cubic Solid Solution Alloys,* École Polytechnique Fédérale de Lausanne, Thesis Nr. 8383 (2018).